

DESY SR 86-01  
January 1986

VALENCE BANDS OF ORIENTED FINITE LINEAR CHAIN MOLECULAR SOLIDS  
AS MODEL COMPOUNDS OF POLYETHYLENE STUDIED BY ANGLE-RESOLVED PHOTOEMISSION

by

K. Seki, N. Ueno, U.O. Karlsson, R. Engelhardt  
*Hamburger Synchrotronstrahlungslabor HASYLAB at DESY*

E.E. Koch  
*Fritz-Haber-Institut der Max-Planck-Gesellschaft, Berlin*

Eigentum der Property of	<b>DESY</b>	Bibliothek library
Zugang: Accessions:	18. MRZ. 1986	
Leihfrist: Loan period:	<b>7</b>	Tage days

ISSN 0723-7979

NOTKESTRASSE 85 · 2 HAMBURG 52

DESY behält sich alle Rechte für den Fall der Schutzrechtserteilung und für die wirtschaftliche Verwertung der in diesem Bericht enthaltenen Informationen vor.

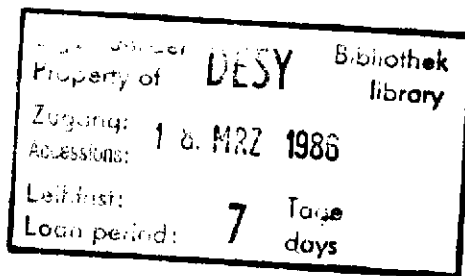
DESY reserves all rights for commercial use of information included in this report, especially in case of filing application for or grant of patents.

To be sure that your preprints are promptly included in the  
HIGH ENERGY PHYSICS INDEX ,  
send them to the following address ( if possible by air mail ) :

DESY  
Bibliothek  
Notkestrasse 85  
2 Hamburg 52  
Germany

Valence Bands of Oriented Finite Linear Chain Molecular Solids as  
Model Compounds of Polyethylene Studied by Angle-Resolved  
Photoemission<sup>1</sup>

K. Seki<sup>2</sup>, N. Ueno<sup>3</sup>, U.O. Karlsson<sup>4</sup>, R. Engelhardt<sup>5</sup>  
Hamburger Synchrotronstrahlungslabor HASYLAB at DESY  
Notkestr. 85, D-2000 Hamburg 52, Germany  
and  
E.F. Koch  
Fritz-Haber-Institut der Max-Planck-Gesellschaft,  
Faradayweg 4-6, D-1000 Berlin 33, Germany



Angle-resolved photoemission spectra were measured using synchrotron radiation of two kinds of oriented model compounds of polyethylene with their molecular axes perpendicular to the substrate surface, i.e. evaporated films of hexatriacontane  $\text{CH}_3(\text{CH}_2)_{34}\text{CH}_3$  and Langmuir-Blodgett films of Cd arachidate  $(\text{CH}_3(\text{CH}_2)_{17}\text{COO})_2\text{Cd}$ . Both films show similar photoelectron energy distribution curves determined by the long-alkyl chain. The intramolecular energy-band dispersion of polyethylene was determined from the photon-energy dependence of the normal-emission spectra. This is the first direct observation of an energy-band dispersions in organic solids. The upper bands formed by C 2p and H 1s electrons extend from 8.8 to 15.5 eV below the vacuum level, and the deeper-lying bands originating from C 2s electrons lie from 17.5 eV to 24.7 eV. The band structure obtained is compared to results from XPS and ESR studies. Furthermore, the experimentally determined band structure is discussed in detail in view of theoretical calculations for polyethylene. Ab initio and extended Hückel calculations give a good description of the experimental results.

<sup>1</sup>Work supported in part by Bundesministerium für Forschung und Technologie (BMFT) from funds for research with synchrotron radiation.

permanent addresses:

<sup>2</sup>Institute for Molecular Science, Myodaiji, Okazaki 444, Japan

<sup>3</sup>Dept. of Image Science and Technology, Faculty of Engineering, Chiba 260, Japan

<sup>4</sup>Dept. of Physics, Linköping University, S-58183 Linköping, Sweden, now at IBM Thomas J. Watson Research Center, Box 218, Yorktown Heights, NY 10598, USA

<sup>5</sup>II. Institut für Experimentalphysik, Universität Hamburg, D-2000 Hamburg 50, Germany

## 1. Introduction

The electronic structure of polyethylene  $(\text{CH}_2)_n$  has been studied extensively, since (i) it is one of the prototype polymers and also a typical quasi-one-dimensional compound, (ii) the elucidation of its electronic structure is the basis for understanding the electronic structure of many derivative polymers (e.g. vinyl polymers), and (iii) such studies may be helpful for clarifying the breakdown mechanism of polyethylene as a widely-used insulating material [1]. On the theoretical side, McCubbin and Gurney [2] first discussed the electronic structure of polyethylene, and virtually all existing versions of band calculations for the valence bands of a polymer chain have been applied to polyethylene as a test polymer to examine their validity [3-41].

On the experimental side, ultraviolet photoelectron spectroscopy (UPS) and X-ray photoelectron spectroscopy (XPS) have been used to elucidate the valence electronic structure. Fujihira and Inokuchi [42] first determined the photoemission threshold of polyethylene by UPS. Wood et al. [16] and Delhalle et al. [22] studied the whole valence band structure by a combination of XPS with theoretical calculations, and assessed that the valence bands consist of upper  $\text{C}_{2p} + \text{H}_{1s}$  bands and deeper-lying  $\text{C}_{2s}$  bands. Further, the formation of an intrachain band from  $\text{C}_{2s}$  orbitals and its insensitivity to the long-range order were clearly demonstrated by the XPS studies of linear alkanes [43,44]. Information on conduction bands and disordered states have also been obtained by UPS [45-47], secondary electron

emission spectroscopy [46,48-50], absorption spectra [51,52], and photoconduction [53,54].

There are, however, still challenging questions related to the valence electronic structure of an isolated planar-zigzag extended chain. Firstly, the photoionization cross section of  $\text{C}_{2p}$  derived bands at XPS energies is small, and the decreased sensitivity hampered a detailed study of the upper  $\text{C}_{2p} + \text{H}_{1s}$  bands, which are more important than the deeper-lying  $\text{C}_{2s}$  bands in discussing the electronic conduction and fundamental photoabsorption. Since UPS is more sensitive to  $\text{C}_{2p}$  derived orbitals and generally yields higher resolution than XPS, a precise study of the valence bands by UPS is highly desirable.

Secondly, UPS and XPS experiments on organic polymers gave so far only information on the density of states (DOS), while theoretical calculations offer more detailed information, e.g. the wavevector,  $\mathbf{k}$ , dependence of the electron energy, the intrachain energy band dispersion relation  $E = E(\mathbf{k})$ . Such energy-band dispersions are now routinely determined for metals, semiconductors, or adsorbed layers by angle-resolved UPS (ARUPS) techniques [55]. In organic solids, the weak van der Waals intermolecular interaction causes only a small intermolecular energy band dispersion of the order of 0.1 eV [56]. This is negligible compared with the large intramolecular dispersion of the order of 5 eV, due to the strong interatomic covalent bond within the chain. So, the determination of an intrachain  $E = E(\mathbf{k})$  dispersion should be possible for an oriented sample. Up to now, however, this technique has not yet been successfully

applied to organic polymers, because of the difficulty in preparing well-oriented samples suitable for ARUPS measurements.

Fortunately, such oriented samples can be obtained for polyethylene by using model compounds with sufficiently long alkyl chains. Normal alkanes constitute one group of such compounds. XPS results [43] and our recent ab-initio MO calculations [57] indicate that a normal alkane  $n\text{-CH}_3(\text{CH}_2)_{n-2}\text{CH}_3$  with  $n \gtrsim 12$  is sufficiently long to simulate the whole valence electronic structure of polyethylene. Alkanes are also largely free from difficulties encountered with a real polyethylene solid, namely the coexistence of crystalline and amorphous regions, chain folding, branching, and incomplete purity [58]. Such factors hamper a meaningful comparison with theoretical calculations. Alkanes can be evaporated to form oriented polycrystalline films, in which fully extended planar zig-zag chains are packed with their molecular axes perpendicular to the substrate surface [45]. A significant angular-dependence of photoemission spectra was actually observed in our previous UPS study of an evaporated film of  $n\text{-CH}_3(\text{CH}_2)_{34}\text{CH}_3$  with a rare-gas resonance line, and the possibility of studying intermolecular band using such an oriented film was suggested [47]. The elucidation of the  $E = E(\mathbf{k})$  relation was hampered, however, since no tunable light source was available.

Another class of excellent model systems of oriented polyethylene are Langmuir-Blodgett films (LB films) consisting of fatty acids and their metal salts. They can be assembled layer by layer to form planar two-dimensional sheets, with the molecular axes perpendicular to the substrate. Since the

compounds forming LB films consist of a hydrophobic long-alkyl chain and a hydrophilic group, they can be regarded as a model of polyethylene when the contribution of the hydrophilic part can be neglected. An almost complete molecular orientation is realized in such films, which is ideal for angle-resolved studies. Furthermore, the elucidation of the electronic structure of such films is interesting in itself, since they have recently attracted interest for developing new types of electronic devices [59,60], two-dimensional magnets [61], and as good models of biological membranes.

In this paper we report on ARUPS studies of (i) oriented films of hexatriacontane  $n\text{-CH}_3(\text{CH}_2)_{34}\text{CH}_3$  prepared by in-situ vacuum evaporation, and of (ii) LB films of a simple carboxylic acid salt Cd arachidate  $(n\text{-CH}_3(\text{CH}_2)_{17}\text{CH}_2\text{COO})_2\text{Cd}$ , using synchrotron radiation as a tunable light source. Both samples showed remarkable spectral changes depending on the photon energy, the incidence angle of the photon beam (E-field vector dependence), and the emission angle of the electrons. In particular from the photon energy dependence we are able to determine the intramolecular  $E = E(\mathbf{k})$  dispersion. These are the first experimental observation of an energy band dispersion in an organic solid, which we have already reported briefly elsewhere [62,63]. In the present paper we will present a more comprehensive study, including more detailed results and a complete comparison with previous XPS spectra and available theoretical band-structure calculations.

## 2. Experimental Procedure

### 2.1. Samples and Measurements

The sample of  $n\text{-C}_{16}\text{H}_{34}$  was supplied by Tokyo Kasei Co. Ltd., and was purified in 3 cycles of recrystallization from benzene solution. The specimen was prepared as a film of  $\sim 7$  nm thickness on a polished Cu substrate by in-situ evaporation in an ultrahigh-vacuum (UHV) preparation chamber (base pressure  $5 \times 10^{-10}$  Torr) and subsequently transferred to the photoelectron spectrometer under UHV. Previous data from (i) X-ray diffraction of thicker evaporated films on Cu [45] and (ii) vacuum-uv absorption spectra from films of comparable thickness on LiF [52] showed that oriented polycrystalline films are formed by evaporation with the molecular axis perpendicular to the substrate surface, as shown in Fig. 1(a).

Three and two monomolecular cadmium salt layers of arachidic acid of Y-type were prepared on aluminium- and gold-covered glass plates, respectively, as shown in Fig. 1(b). The method for film preparation is described in Ref. [64]. For both cases, the sample surface was covered by the oriented hydrocarbon chains. The subphase (Millipore water pH 5.5) contained  $4 \times 10^{-4}$  M  $\text{CdCl}_2$ . Thus the Cd salt is deposited on the support giving the film a good stability. These samples were prepared and kindly given to us by H. M $\ddot{o}$ hwald. We note that the conformation of the alkyl chain in both hexatriacontane and Cd arachidate is essentially the same as that of polyethylene crystals [65] shown in Fig. 1(c).

Photoelectron spectra were measured for various angles of

incidence  $\alpha$  of the photon beam, polar emission angles  $\theta$  of the electrons and azimuthal emission angles  $\phi$  of the electrons (see Fig. 2(a)) with an

apparatus at the storage-ring DORIS II in the Synchrotron Radiation Laboratory HASYLAB at DESY [66]. The setup consists of a 1 m Seya-Namioka type monochromator and a modified VG ADES 400 angle-resolving photoelectron spectrometer. The light intensity impinging on the sample was monitored by measuring the photoemission from an Au-coated diode placed between the exit slit of the monochromator and the sample. Prolonged illumination with intense light caused a change of the spectra for both compounds, which is probably due to radiation damage. In order to avoid this, the intensity was kept low with narrow slit width. Furthermore, the spectra were recorded with frequent changes of the sampling position on the specimen. The absence of damage was confirmed by remeasuring spectra for a fixed combination of  $h\nu$ ,  $\alpha$ ,  $\theta$ , and  $\phi$  after several runs. By such a careful procedure, spectra amenable for subsequent analysis were obtained.

### 2.2. Band Structure Mapping by $h\nu$ -dependent Normal Emission

In this section we will briefly describe the method of energy-band mapping by ARUPS used in the analysis of our data. For a detailed description, see Ref. [55].

Usually the photoemission process is treated in a three-step (photoexcitation, transport, and emission through the surface) model [67]. Further, we make the following two basic assumptions:

PHOTOEXCITATION (energy and momentum conservation):

$$E_f = E_i + h\nu, \quad \hbar k_f = \hbar k_i + \mathcal{G} \quad (1)$$

EMISSION (energy and momentum conservation for escape process):

$$E_{kin} = E_f, \quad \hbar k^{\parallel} = \hbar k_f^{\parallel} + \mathcal{G}^{\parallel} \quad (2)$$

where  $E_i$ ,  $E_f$ ,  $k_i$  and  $k_f$ , are the energy and the wave vector of the electron before and after photoexcitation in the solid,  $E_{kin}$  and  $k$  are the energy and wavevector of the emitted free electron, and  $\mathcal{G}$  is the reciprocal lattice vector. The component parallel to the surface is denoted by  $\parallel$ . All the energies are measured from the vacuum level.

Equation (1) shows that the transition is direct, i.e. both the energy and momentum of the excited electron must be conserved for the transition (see Fig. 2(b)). The conservation of  $k$  results from the negligible momentum of the exciting photon. Equation (2) indicates that the parallel component of the wavevector should be conserved on crossing a smooth surface, because of the absence of any abrupt change in the potential along the surface.

Using these equations and assuming a known final state dispersion  $E_f = E_f(k)$  (see Fig. 2b and below), one can obtain the initial state dispersion  $E_i = E_i(k)$  by tuning  $h\nu$ . Assuming a rather crude but successful approximation [55], we use a free-electron-like parabola as the final-state dispersion curve at higher energies.

The relation between the kinetic energy and the wavevector of a free electron in the vacuum is expressed as

$$E_{kin} = \hbar^2 k^2 / 2m = \hbar^2 (k^{\parallel 2} + k^{\perp 2}) / 2m. \quad (3)$$

On the other hand, the corresponding relation in the solid is

different due to the potential in the solid. For the final state, we assume the following relation for a nearly-free electron in a constant inner potential in the solid  $V_0$ :

$$E_f = \hbar^2 k_f^2 / 2m + V_0 = \hbar^2 (k_f^{\parallel 2} + k_f^{\perp 2}) / 2m. \quad (4)$$

For normal emission,  $k^{\perp} = 0$ , hence  $k_f^{\perp} = k_i^{\perp} = 0$ .

Accordingly, the following relations can be derived:

$$\hbar k_i^{\perp} = \hbar k_f^{\perp} = \sqrt{2m (E_k - V_0)} / \hbar, \quad (5)$$

$$E_i = E_{kin} - h\nu. \quad (6)$$

These relations indicate that the values of  $E_i$  and  $k_i^{\perp}$  can be determined from the measured  $E_{kin}$  and  $h\nu$ , provided  $V_0$  is known. Since  $k_i$  changes with the change of  $h\nu$  to fulfill Eq. (1), we can probe the energy band dispersion  $E_i = E_i(k_i)$  by the  $h\nu$ -dependence of normal-emission spectra. In the present case, this direction is parallel to the molecular axis along which intramolecular interaction is expected to be strongest. Since the interaction between different chains is weak, the dispersion should be dominated by this intramolecular interaction.

### 3. Experimental Results, Wide Scan Spectra

In Fig. 3, examples of the photoelectron spectra of  $n$ - $\text{CH}_3(\text{CH}_2)_{34}\text{CH}_3$  for normal emission ( $\theta = 0^\circ$ ) and  $h\nu = 22$  to 45 eV are shown on the kinetic energy ( $E_{kin}$ ) scale. Similar spectra were obtained for LB films, indicating that the spectra are dominated by the contribution from the alkyl chains. Electrons emitted without inelastic scattering (primary electrons) form the peaks at large kinetic energies. They reflect the structure of the valence bands. The 2p electrons of C and 1s electrons of H

form the upper bands, and the  $C_{2s}$  orbitals form deeper-lying bands [16,22], as shown in the figure. They will be discussed in the following sections. The intense features observed in the photoelectron spectra at  $E_{kin} \leq 8$  eV are due to secondary electrons produced by inelastic scattering.

The intensity ratio of the primary electrons ( $I_p$ ) to secondaries ( $I_s$ ) increases rapidly with  $h\nu$ . (Spectra at  $h\nu \leq 20$  eV show smaller  $I_s/I_p$  ratios [45]). This change is due to strong inelastic scattering of primary electrons via electron-electron scattering. The threshold kinetic energy of this process can be estimated as  $E_{kin} = E_x - E_A$ , where  $E_x$  and  $E_A$  are the lowest electronic excitation energy and electron affinity, respectively. With reported values  $E_x = 7.5$  eV [52] and  $E_A \sim 0$  eV [68], we obtain a threshold of  $E_{kin} = 7.5$  eV. This means that the primaries just start to be attenuated at  $h\nu = 22$  eV, and the growing effect of scattering increases the  $I_s/I_p$  ratio rapidly.

In the region  $E_{kin} \lesssim 8$  eV, the photoelectron spectra have structures at energies independent of  $h\nu$ , as already observed in angle-integrated UPS measurements [45,46] and secondary-electron emission measurements [46,50]. These features reflect the density of unoccupied states [45,46], and will be discussed in detail elsewhere [69]. In the following we will concentrate on discussing the primary electron emission reflecting the valence band structure.

#### 4. Angular Dependence of Photoemission from the Valence-Bands and Molecular Orientation

Drastic changes in the energy distribution curves are

observed by varying  $\alpha$  and  $\theta$ . For both compounds no  $\phi$ -dependence of the spectra was found. The insensitivity to  $\phi$  is reasonable when we consider that the sample films consist of microdomains with random azimuthal orientation (for LB films, see Ref. [70]).

In Fig. 4(a), the  $\alpha$ -dependence of the normal-emission spectra plotted on a binding energy scale for hexatriacontane at  $h\nu = 38$  eV, is shown. In the  $C_{2p} + H_{1s}$  bands, two peaks A and C appear. In the  $C_{2s}$  range, a peak labelled D is observed. Assuming a fixed vertical orientation of the molecules with respect to the surface, a change of  $\alpha = 15^\circ$  to  $\alpha = 70^\circ$  corresponds to changing the angle between the electric vector of the polarized synchrotron radiation and the molecular axis. (see the insert in Fig. 4(a)). A drastic change of the relative emission intensity with  $\alpha$  can be seen. The  $\theta$ -dependence for  $h\nu = 38$  eV and  $\alpha = 70^\circ$  is shown in Fig. 4(b). The small shift of the peak positions can be qualitatively understood by  $E = E(k)$  dispersion. Similar  $\alpha$ - and  $\theta$ -dependences were also observed for the LB films.

Such large  $\alpha$ - and  $\theta$ -dependences reflect the good orientation of the molecules. Further support for high degree of orientation comes from thermally induced disorder. The heat-treated sample did not show such a clear  $\alpha$ - and  $\theta$ -dependence of the spectra as observed for ordered films (see Figs. 4(a) and (b)). For example, Fig. 5 clearly demonstrates the loss of angular dependence of the photoemission signal from heat-treated LB films, e.g. for  $\theta = 0^\circ$  the relatively intense peak D loses its intensity, and the intensity does not recover after cooling. A similar disappearance of anisotropy was also observed in the  $\alpha$ -dependence of the



spectra. These observations concur with the results from X-ray diffraction which show that the molecular orientation in the LB film of Cd arachidate is destroyed by heating above 100 °C and that the molecular orientation does not recover after cooling [71]. Thus we conclude that the large angle (both  $\alpha$  and  $\theta$ ) dependence of the spectrum is the result of the good orientation of the molecules. We note here in passing that one can check the molecular orientation of sensitive samples by in-situ ARUPS measurements as described above even for compounds for which electron diffraction measurements produce severe radiation damage followed by destruction of the molecular orientation.

From the above observation, we note that the intensity ratio of peak D to peak A in normal emission can be used as an index of the degree of orientation. Thus a 3-layer LB film showed better orientation than a 2-layer LB film or even evaporated n-C<sub>36</sub>H<sub>74</sub> as shown in Fig. 4(c). This can be understood as follows: (1) an imperfect surface of the substrate perturbs the orientation at the first layer, (2) the second layer shows a better orientation since it is deposited on the already oriented first layer, and (3) the third layer shows a still better orientation owing to the well-oriented 2nd layer, and so on. Our observation is supported by recent results from Penning ionization electron spectroscopy on LB films of anthraquinone derivatives [72].

For the moment we cannot analyze the intensity variation with  $\alpha$  and  $\theta$  in detail, but these experimental data will serve as a good test for future theories of angular-dependent photoemission from oriented molecules. For such theoretical studies, the C<sub>2s</sub> peak will be particularly suitable because of its simple character discussed in section 7.

## 5. $h\nu$ -Dependence of Normal Emission

The  $h\nu$ -dependence of the spectra of hexatriacontane for photoelectrons emitted normal to the surface at  $26 \text{ eV} \leq h\nu \leq 54 \text{ eV}$  is shown in Fig. 6. The spectra show changes both in peak positions and peak intensities of the main features. In the C<sub>2p</sub> + F<sub>1s</sub> bands, two peaks A and C appear for  $h\nu \lesssim 40 \text{ eV}$ , as described above. For  $h\nu \gtrsim 40 \text{ eV}$ , a new peak labelled B appears. Peak B shifts toward higher binding energies with increasing photon energy. Peak C merges into it. In the C<sub>2s</sub> range, a sharp peak labelled D, which was also mentioned above, is observed. Its position changes slowly to higher binding energies with increasing  $h\nu$ .

In Fig. 7, we show the corresponding data for a two-monolayer Cd arachidate film. The results are essentially similar to those in Fig. 6. This again indicates that the spectra are dominated by the contribution from the alkyl chain and not affected appreciably by the COO<sup>-</sup> or Cd<sup>2+</sup> parts. This is most probably due to the short electron mean free path ( $\leq 10 \text{ \AA}$ ) [73] in the present energy range compared to the length of the alkyl part ( $\sim 23 \text{ \AA}$ ) in a Cd arachidate molecule and also due to the 214 to 42 ratio of valence electrons involved in the alkyl and the rest parts of the molecule, respectively.

Furthermore, Fig. 7 clearly shows the  $h\nu$ -dependence of the whole C<sub>2s</sub> band. In addition to peak D, two features are visible labeled D' and E. The peak energy of peak E in Fig. 7 shifts towards lower binding energy by increasing  $h\nu$ . The weak shoulder

$D'$  remains at an almost constant energy position independent of  $h\nu$ . The intensity of feature  $D'$  depends on the position of the sample monitored and on the history of the sample. After intense VUV light irradiation it increases, while the intensity of feature  $D$  decreases. We thus assume that the feature  $D'$  originates from the photoemission of defects created in the film. This


could be emission from misaligned chains resulting from a destruction of the polar head groups, which was observed in XPS experiments [74]. This idea is also supported by the absence of a corresponding feature in the spectra of irradiated hexatriacontane.

In addition to peak positions also the intensities of spectral features in Figs. 6 and 7 depend significantly on  $h\nu$ . This will be discussed in the next section.

## 6. Intramolecular Energy-Band Mapping

For a determination of  $E = E(k)$  energy band from the spectra in Figs. 6 and 7, we follow the procedure as described in section 2.2. The value of  $V_0$  can be determined from the  $h\nu$ -dependence of the photoemission intensity of the upper  $C_{2s}$  band  $D$  shown in Fig. 8. The intensity shows a maximum when the energy matches the energy separation between the  $C_{2s}$  valence band and the nearly-free electron parabola at the  $\Gamma$  point. In the lower part of Fig. 9, we show the  $E_i = E_i(k_i)$  relation by an ab-initio calculation [38], which is a little modified as described below. We can easily ascribe the peak  $D$  to the flat band around  $E_i = -18$  eV. As shown

in Fig. 9, we assign the maximum at  $h\nu = 36$  eV to a large joint DOS for the transition at the  $\Gamma$  point [75] due to the flatness of the nearly-free electron final-state bands at the  $\Gamma$  point [76]. From this,  $V_0$  can be determined to be -5.5 eV, and we obtain an  $E_f = E_f(k_f)$  relation shown in the upper part of Fig. 9. Note that the bottom part (indicated with broken lines) of the final band cannot be approximated by a nearly-free-electron parabola due to the effect of the potential in the solid. Thus only the region above  $E_f \sim 10$  eV was used for the subsequent analysis.

The experimental band structure obtained in this way is shown in Fig. 10. As a guide for the eye, results of an ab-initio calculation for a polyethylene chain by Karpfen [38] are also shown. For a better fit with the experimental data, the original calculated band structure was 0.8 times contracted and shifted in energy scale. This dispersion relation of the occupied states was also used for Fig. 9.  The symmetries of the bands are taken from Ref [18a]. We note that the corresponding figure for  $n\text{-CH}_3(\text{CH}_2)_{34}\text{CH}_3$  in the rapid communication [62] was in error for the width of the Brillouin zone by 7 %, but the main features of the diagram and conclusions are not affected by this. The energy band structure shown in Fig. 10 is the most detailed <sup>experimental</sup> information on the valence electronic structure of a polymethylene chain. Therefore, in the following sections we will compare the results with other available from XPS, ESR, and with theoretical calculations.

In passing we note that the  $h\nu$ -dependence of the peak intensities in Figs. 6 and 7 can also be understood quantitatively with the help of the electron band structure. For example, the

decrease of the intensity of peak D between 46 and 54 eV

is predicted by calculating the joint density of states using values read from the figures in Karpfen's paper for the initial states. However, for a more detailed comparison, the joint density of states has to be calculated quantitatively.

## 7. Comparison with XPS results

Several XPS studies of the valence band of polyethylene and its model compounds have been performed [22,42-44,77]. In these studies, the  $C_{2s}$  band has been investigated in quite detail, because of its large photoionization cross section. On the other hand, the study of the  $C_{2p} + H_{1s}$  band was much more difficult due to the small cross section in XPS. Nonetheless, a detailed XPS study of the whole valence band for highly crystalline polyethylene [22] has served for the comparison with theoretical calculations [18-24,28-31,33,35,38]. In Fig. 11 this spectrum (solid line in (c)) is compared with the present UPS results ((a) and (b)). Since the XPS spectrum reflects largely the density of initial states, we have chosen several ARUPS spectra at different  $h\nu$  for which the peak energies correspond to flat portions of the energy bands giving large DOS. In (b), we also show an angle-integrated spectrum of 2-layer LB film <sup>obtained with a</sup> He II light source [78]. The XPS spectrum was shifted to align the upper  $C_{2s}$  peak (D), since the original energy scale is relative to the Fermi level. This corresponds to a work function of 4.8 eV, which is close to the value of 4.5 eV determined in the previous UPS experiments [42]. The peak positions are listed in Table 1, with

other relevant data.

There is a rough correspondence between the UPS and XPS spectra. The large difference in relative peak intensities of the  $C_{2p} + H_{1s}$  and  $C_{2s}$  bands is due to the different  $h\nu$ -dependences of the photoionization cross sections. As for the  $C_{2s}$  band, the agreement of the peak energies is good.

However, we also note that there are several significant differences: (i) binding energies for peak B and C do not agree. (ii) The minimum between the  $C_{2p} + H_{1s}$  and  $C_{2s}$  bands is far more pronounced in our UPS data, furthermore its energetic separation from the  $C_{2s}$  maximum is quite different. (iii) The shoulder labelled X in the XPS spectrum is not observed in our UPS spectra. As already mentioned, the difference in the carbon number should not cause such significant differences [43,57]. For (i) and (ii), we believe that our results are more reliable. Firstly, the signal-to-noise ratio in the present UPS study is better than that in the XPS spectrum. Secondly, the present UPS results agree with the XPS spectrum of  $n-C_{36}H_{74}$  by Pireaux et al. [43,77] (broken line in Fig. 11(c)), which was reported without discussing the  $C_{2p} + H_{1s}$  band. Point (iii), will be discussed in section 8.1.

Finally we note that the simple nature of the  $C_{2s}$  band allows us to compare the  $E = E(k)$  relation in Fig. 10 with the previous XPS studies of the  $C_{2s}$  band formation by Pireaux et al. [43,44]. The latter authors clearly demonstrated that the  $C_{2s}$  level of methane is split into many levels in longer alkanes, a result which agreed well with ab-initio calculations. By

assuming a tight-binding model for a 1-dimensional array with nearest-neighbor interaction, we can assign a value of  $k$  to each of such split levels as [79]

$$k = (2/am)/(n+1), \quad (7)$$

where  $n$  is the number of carbon atoms, and each  $m$  corresponds to a pair in the upper and lower branch of split levels ( $m$  runs from 1 to the maximum integer not exceeding  $(n + 1)/2$ ). Such a treatment was successfully applied to a detailed analysis of the valence electronic structure of poly-p-phenylene [80]. In Fig. 12 the results of Pireaux et al. for (a)  $n = 1$  to 5 (gas) and (b)  $n = 5$  to 9 (solid) are plotted in this way. The absolute energy scale was adjusted to give the best fit with our present UPS data. We see a close agreement between the data from oligomers with the present directly-measured results. This agreement indicates that the simple assumption of the nearest-neighbor interaction works reasonably well in the case of the  $C_{2s}$  band.

#### 8. Comparison with theoretical calculations.

Most methods for band structure calculations have been applied to polyethylene as a standard polymer system. So it will be useful to make an extensive comparison of the present results with various calculations to examine their validity. A comprehensive comparison of the numerical results is presented in Table 2. In addition, in Fig. 13, representative calculated  $E = E(k)$  diagrams are compared with the present experimental results (points in Fig. 13(a) and (e)). Note that the energy scale of the experimental data is shifted to show a better agreement with

calculations, as shown in the right ordinate of Fig. 13(a) and (e). Finally the density of states obtained from these calculations are compared with the UPS and XPS spectra in Fig. 14.

Before we make a detailed comparison of the observed and theoretical results, two remarks are in order. Firstly, there is a difference due to the state of aggregation, between the observed solid state photoelectron spectra and theoretical calculations on an isolated chain. However, it is known that the photoelectron spectrum of a molecular van der Waals solid agrees well with that of the constituent molecule when we allow for a rigid shift in the energy scale (solid state relaxation energy) [81-84], which mainly arises from the electronic polarization of the surrounding molecules in the solid (see e.g. Ref. [56,84,85]). Fortunately, a detailed comparison with the photoelectron spectra of  $n-C_{36}H_{74}$  in the gas phase, which will be reported separately [57], indicates that such a shift is of the order of 0.5 eV or so in the present case, which is not significant for our comparison. Hence we can directly compare the observed and calculated results by adjusting the energy scales.

Secondly, many early calculations used a wrong molecular geometry or failed in taking properly into account symmetry requirements, such as the repulsion of the bands of the same symmetry or the pairing of bands at the boundary of the Brillouin-zone (X-point). We have indicated such problems in the calculation in Table 2.

## 8. 1. Ab initio calculations

At first we will compare the observed results with the ab initio calculation by Karpfen [38], since (i) it was claimed to reach almost the Hartree-Fock limit, (ii) the correct experimental geometry was used, (iii) the effects of choosing the optimum basis set was carefully assessed, and (iv) the degree of nearest neighbor—second nearest neighbor—etc.—interactions among  $-\text{CH}_2\text{CH}_2-$  units is extrapolated to infinity. Figs. 10 and 13(a) are convenient for this comparison.

The calculated ionization potential (top of the valence band) 10.0 eV is in a fair agreement with the vertical ionization potential of 9.8 eV for the gas phase estimated from the experimental data [57]. The remaining difference may be ascribed to the assumption of Koopmans' theorem. We note, however, that the uppermost  $B_1$  band at  $k = 0$ , which forms the top of the valence bands according to the calculation, was not observed separately from peak A, as already stated in section 6. Even around  $h\nu = 27$  eV, where  $h\nu$  is expected to match the excitation energy from this band to the free-electron-like final state at the  $\Gamma$  point (see Fig. 9), we could not observe a separate peak. Thus we are unable to confirm the observation of a weak shoulder labelled X in Ref. [22] (see Fig. 11(c)). One might speculate that the  $B_1$  band actually does not form the top of the valence band. However, detailed ESR studies of long-alkane cation by Toriyama et. al. [86] clearly demonstrate that the ground state of a long-alkane cation is the  $B_1$  state. So, we tentatively

ascribe this disappearance to the combination of three factors: (i) The solid-state broadening of each energy level ( $\sim 0.6$  eV FWHM) [84,87,88], (ii) the calculated energy separation between  $B_1$  and  $A_1/A_2$  bands at the  $\Gamma$  point is too large, and (iii) blurring of the peak in the DOS by electron-phonon coupling upon ionization, which is expected to be significant in quasi-1-dimensional systems [89]. Such a broadening will make it difficult to distinguish a weak feature at the top of the valence band from the closely-located intense feature A. In passing, we note that the highest occupied states of n-alkanes (except for methane) are not degenerate, in contradiction to the argument in Ref. [33] that a Jahn-Teller splitting of this degeneracy is a possible origin of the broadening of photoelectron spectra.

For deeper levels, the contracted-and-shifted ab initio results describe the experimental data very well. In particular, the dispersion of the upper  $B_1$  band and the lower  $A_1$  band around the middle of the Brillouin-zone is clearly observed in the experiment.

Karpfen pointed out that (i) the discrepancy due to Koopmans' theorem should become progressively larger when one goes to higher ionization energies and that (ii) the Hartree-Fock energy band will be too broad as a consequence of this effect. The present results clearly show that Karpfen's idea was correct. The apparent contradiction between this theoretical expectation [38] and previous bandwidth derived from XPS can be ascribed to an ambiguous determination of the bottom of the  $C_{25}$  bands from experimental data.

As seen in Table 2, other ab-initio calculations also give

reasonable results. We note that the introduction of the equivalent-core-potential (ECP) approximation does not change the dispersion relation significantly [40].

### 8. 2. Semiempirical SCF-LCAO MO calculations

As seen in Fig. 13, original versions of semiempirical MO calculations such as CNDO (Complete Neglect of Differential Overlap), CNDO/2, INDO (Intermediate Neglect of Differential Overlap), MNDO (Modified Neglect of Diatomic Overlap), MINDO (Modified INDO)/2, and MINDO/3 give too large total band widths due to the neglect of differential overlap of electrons. MNDO (Fig. 13(d)) [33] gives a reasonable description of the  $C_{2p} + H_{1s}$  band, except that the ionization potential is a little too large.

On the other hand, Fig. 13(b) and (c) indicate that the CNDO method can be modified to give a moderately good overall agreement with experiment concerning band widths (both  $C_{2p} + H_{1s}$  and  $C_{2s}$  bands) and the absolute energy scale. Based on this observation, we question the argument of Dewar et al. [33] that the too large  $C_{2s}$  band width of MNDO calculation is due to the neglect of 1s-2s interactions.

### 8. 3. Extended Hückel Method

It is noteworthy that this oldest band calculation on polyethylene [3], which is also quite simple, gives good results, as seen in Fig. 13(e), except that the binding energies are too

large. Its calculated band widths and the  $E = E(k)$  dispersion are almost the same as those by ab initio calculation. These facts show the usefulness of this simple method for quantitative band calculations of saturated-hydrocarbon compounds and polymers.

### B. 4. Other methods

The SAMO (Simulated Ab-initio Molecular Orbital), LCLO (Linear Combination of Localized Orbitals) and FSGO (Floating Spherical Gaussian Orbitals) methods are nonempirical methods, which were developed to simulate ab initio calculations and to save computer time, by using the transferability of the matrix elements of HF equations or localized orbitals from simple model molecules. As we can see from Fig. 13, the results of these methods indeed simulate the ab initio results and experimental results. The LCLO result is a little better in reproducing the dispersion in the  $C_{2p} + H_{1s}$  band. The FSGO method (Fig. 13(f)) gives too large binding energies, but the contraction of the energy scale by 0.7 time offers reasonable results [35].

In contrast to these, the techniques using local exchange, such as LCAO-MT (Muffin Tin), EMTO (Extended Muffin Tin Orbitals) and DV- $X_\alpha$  methods give rather poor agreement with experimental observations. The width of the  $C_{2p} + H_{1s}$  bands given by the LCAO-MT method (Fig. 13(g)) is too large. The EMTO and DV- $X_\alpha$  methods fail in placing the  $B_1$  band at the top of the valence band at  $k = 0$ . Further, the bands in the reported EMTO calculation do not lie horizontally at  $k = 0$ .

These poor results are not surprising when we consider that

these calculations are still not yet well developed for dealing with organic molecular systems. Clearly some basic improvements are necessary for applying these techniques to organic solids.

#### 9. Concluding Remarks

In this paper we have reported on a detailed study of angle-resolved photoelectron emission from oriented samples of hexatriacontane and Cd arachidate, which are good models of polyethylene in an extended-chain conformation. It was possible to determine intramolecular quasi-one-dimensional  $E = E(k)$  energy band dispersion for the valence bands from the photon energy dependence of normal emission spectra. In fact, this is the first experimental observation of an  $E = E(k)$  energy band dispersion in an organic solid. In particular, information concerning the upper  $C_{2p} + H_{1s}$  valence band is much more precise than that from the previous XPS data. This allowed us a detailed comparison with theoretical band structure calculations.

Our experimental results in comparison with the many partly conflicting theoretical calculations stress the importance of polyethylene as a test material for the different methods of polymer-band calculations. It is encouraging that the most sophisticated ab-initio calculation [38] gives the best agreement. Semiempirical methods, some with proper modifications, give <sup>also</sup> reasonably good agreement. Among them we note the success of the simple extended-Hückel method.

The present study established the technique of intramolecular-band-mapping by angle-resolved photoelectron

spectroscopy via  $h\nu$ -dependence of normal emission. Furthermore, it clarified the electronic valence band structure of polyethylene. A determination of the intramolecular  $E = E(k)$  dispersion is also possible by angle-resolved UPS from samples with the axes uniaxially oriented parallel to the surface [90], or by measuring the DOS of oligomers [80], a technique which was also applied here to the polyethylene  $C_{2s}$  band. Generally, angle-resolved UPS techniques can be applied to all polymers provided adequately oriented samples are available. Unfortunately this is not always the case, and we must stress the importance of obtaining such specimens. The "oligomer DOS" technique can be applied only to compounds with simple bands, but we can use non-oriented samples and a sophisticated angle-resolved instrument is not even necessary. We anticipate that the application of these complementary techniques will clarify the electronic structures of other organic compounds.

#### Acknowledgements

We are grateful to Prof. Dr. H. Möhwald and Dipl.-Phys. L. Laxhuber of Technische Universität München for kindly providing the LB films, and to Dipl.-Phys. R. Dudde and W. Gädeke of Universität Hamburg for their help during the UPS measurements of LB films. We also acknowledge the continuous and efficient support of the technical staff of HASYLAB. K. Seki, N. Ueno, and U. Karlsson thank DESY, Alexander von Humboldt Stiftung, and DAAD, respectively, for financial support. K. S. and N. U. also thank Prof. H. Inokuchi of the Institute for Molecular Science for his continuous interest and constant encouragement. N. U. gratefully acknowledges the encouragement by Profs. K. Watanabe and K. Sugita of Chiba University.

#### References

- [1] For example, A. R. Blythe, *Electrical Properties of Polymers* (Cambridge University Press, Cambridge, 1979).
- [2] W. L. McCubbin and I. D. C. Gurney, *J. Chem. Phys.* 43 (1965) 483; W. L. McCubbin, *Phys. Stat. Sol. B*16 (1966) 289.
- [3] W. L. McCubbin and R. Manne, *Chem. Phys. Letters* 2 (1968) 230.
- [4] J.-M. André and G. Leroy, *Chem. Phys. Letters* 5 (1970) 71.
- [5] K. Morokuma, *Chem. Phys. Letters* 6 (1970) 186.
- [6] A. Imamura, *J. Chem. Phys.* 52 (1970) 3168.
- [7] H. Fujita and A. Imamura, *J. Chem. Phys.* 53 (1970) 4555.
- [8] J.-M. André, G. S. Kapsomenos, and G. Leroy, *Chem. Phys. Letters* 8 (1971) 195.
- [9] K. Morokuma, *J. Chem. Phys.* 54 (1971) 962.
- [10] E. Clementi, *J. Chem. Phys.* 54 (1971) 2492.
- [11] G. Morosi and M. Simonetta, *Chem. Phys. Letters* 8 (1971) 358.
- [12] W. L. McCubbin., *Chem. Phys. Letters* 8 (1971) 507.
- [13] D. L. Beveridge, I. Jano, J. Ladik, *J. Chem. Phys.* 56 (1972) 4744.
- [14] J.-M. André, J. Delhalle, G. Kapsomenos, and G. Leroy, *Chem. Phys. Letters* 14 (1972) 485.
- [15] B. J. McAloon and P. G. Perkins, *J. Chem. Soc. Faraday* 2 (1972) 1121.
- [16] M. H. Wood, M. Barber, I. H. Hillier, and J. M. Thomas, *J. Chem. Phys.* 56 (1972) 1788.
- [17] B. J. Duke and B. O'Leary, *Chem. Phys. Letters* 20 (1973) 459.
- [18] (a) J. E. Falk and R. J. Fleming, *J. Phys. C*6 (1973) 2954.  
(b) J. E. Falk and R. J. Fleming, *J. Phys. C*8 (1975) 627.



- [19] J. M. André, J. Delhalle, S. Delhalle, R. Caudano, J. J. Pireaux, and J. J. Verbist, *Chem. Phys. Letters* 23 (1973) 206.
- [20] D. L. Beveridge and W. Wun, *Chem. Phys. Letters* 18 (1973) 570.
- [21] M. J. S. Dewar, H. Suck, and P. K. Weiner, *Chem. Phys. Letters* 29 (1974) 220.
- [22] J. Delhalle, J. M. André, S. Delhalle, J. J. Pireaux, R. Caudano, and J. J. Verbist, *J. Chem. Phys.* 60 (1974) 595.
- [23] J. Delhalle, S. Delhalle, and J.-M. André, *Chem. Phys. Letters* 34 (1975) 430.
- [24] S. Delhalle, J. Delhalle, Ch. Demanet, and J. M. André, *Bull. Soc. Chim. Belg.* 84 (1975) 1071.
- [25] W. L. McCubbin, in *Electronic Structure of Polymers and Molecular Crystals* ed, J.-M. Andre and J. Ladik, (Plenum, N. Y. 1975) p. 659.
- [26] P. N. Dyachkov, A. A. Levin, *Theoret. Chim. Acta* 36 (1975) 181.
- [27] P. N. Dyachkov, N. V. Iosolovich, and A. A. Levin, *Theoret. Chim. Acta* 40 (1975) 237.
- [28] G. Leroy, D. Peeters, and F. Rosoux-Clarisse, *Bull. Soc. Chim. Belg.* 85 (1976) 629.
- [29] J. Delhalle, J.-M. André, S. Delhalle, C. Pivont-Malherbe F. Clarisse, G. Leroy, and D. Peeters, *Theor. Chim. Acta* 43 (1977) 175.
- [30] M. J. S. Dewar, Y. Yamaguchi, and H. Suck, *Chem. Phys. Letters* 50 (1979) 259.
- [31] D. R. Armstrong, J. Jamieson, and P. G. Perkins, *Theor. Chim. Acta* 50 (1978) 193.
- [32] W. L. McCubbin, in *Quantum Theory of Polymers*, ed. J. -M. Andre, J. Delhalle, and J. Ladik (Reidel, Dordrecht, 1978) p. 185.
- [33] M. J. S. Dewar, Y. Yamaguchi, and H. Suck, *Chem. Phys.* 43 (1979) 145.
- [34] P. G. Perkins, A. K. Marwaha, and J. P. Stewart, *Theor. Chim. Acta* 57 (1980).
- [35] J. L. Bredas, J. M. André, and J. Delhalle, *Chem. Phys.* 45 (1980) 109.
- [36] D. R. Armstrong, J. Jamieson, and P. G. Perkins, *Theor. Chim. Acta* 57 (1980) 43.
- [37] R. V. Kasowski, W. Y. Hsu, and E. B. Caruthers, *J. Chem. Phys.* 72 (1980) 4896.
- [38] A. Karpfen, *J. Chem. Phys.* 75 (1981) 238.
- [39] R. S. Weidman, K. L. Bedford, and A. E. Kunz, 39 (1981) 917.
- [40] H. Teramae, T. Yamabe, and A. Imamura, *Theor. Chim. Acta* 64 (1983) 1.
- [41] C. Statoko, private communication.
- [42] M. Fujihira and H. Inokuchi, *Chem. Phys. Letters*, 17 (1972) 554.
- [43] J. J. Pireaux, S. Svensson, E. Basilier, P.-A. Malmqvist, U. Gelius, R. Caudano, and K. Siegbahn, *Phys. Rev. A* 14 (1976) 2133.
- [44] J. J. Pireaux and R. Caudano, *Phys. Rev. B* 15 (1977) 2242.
- [45] K. Seki, S. Hashimoto, N. Sato, Y. Harada, K. Ishii, H. Inokuchi, and J. Kanbe, *J. Chem. Phys.* 66 (1977) 3644.

- [46] N. Ueno, T. Fukushima, K. Sugita, S. Kiyono, K. Seki, and H. Inokuchi, *J. Phys. Soc. Jpn.* 48 (1980) 1254.
- [47] K. Seki and H. Inokuchi, *Chem. Phys. Letters*, 89 (1982) 268.
- [48] N. Ueno and K. Sugita, *Jpn. J. Appl. Phys.* 18 (1979) 2159.
- [49] N. Ueno and K. Sugita, *Solid State Commun.* 34 (1980) 355.
- [50] N. Ueno, K. Sugita, and S. Kiyono, *Chem. Phys. Letters* 82 (1981) 296.
- [51] R. H. Partridge, *J. Chem. Phys.* 45 (1966) 1685.
- [52] S. Hashimoto, K. Seki, N. Sato, and H. Inokuchi, *J. Chem. Phys.* 76 (1982) 163, and references therein.
- [53] K. J. Less and E. G. Wilson, *J. Phys. C6* (1973) 3110.
- [54] I. Kitani, K. Yoshino, and Y. Inuishi, *Jpn. J. Appl. Phys.* 19 (1980) 765.
- [55] See e.g. F. J. Himpsel and N. V. Smith, in *Handbook on Synchrotron Radiation*, vol. 1b, ed. E. E. Koch (North-Holland, Amsterdam, 1983) p.905; F. J. Himpsel, *Adv. Phys.* 32 (1983) 1.
- [56] M. Pope and C. E. Swenberg, *Electronic Processes in Organic Crystals* (Clarendon Press, Oxford, 1982).
- [57] K. Seki, N. Sato, and H. Inokuchi, unpublished.
- [58] See, for example, *Macromolecules*, eds. F. A. Bovey and F. H. Winslow (Academic Press, New York, 1979).
- [59] G. G. Roberts, K. P. Pande, and W. A. Barlow, *IEE Solid State Electron Devices* 2 (1978) 169.
- [60] J. H. McAlean and J. M. Wehrung, *Digest of Tech. Papers 1981, Symp. on VLSI Technology* (1981) p.82.
- [61] M. Pomerantz, F. H. Dacol, and A. Segmuller, *Phys. Rev. Lett.* 40 (1978) 246; M. Pomerantz and R. A. Pollack, *Chem. Phys. Lett.* 31 (1975) 602.
- [62] K. Seki, U. Karlsson, R. Engelhardt, and E. E. Koch, *Chem. Phys. Letters* 103 (1984) 343.
- [63] N. Ueno, W. Gädeke, E. E. Koch, R. Engelhardt, R. Dudde, L. Laxhuber, and H. Möhwald, *J. Molec. Electronics*, 1 (1985) xxx.
- [64] H. Kuhn and D. Mobius, *Angew. Chem.* 83 (1971) 672; L. Laxhuber, H. Möhwald, and M. Hashmi, *Int. J. Mass Spectrom. Ion Phys.* 51 (1983) 93.
- [65] C. W. Bunn, *Trans. Faraday Soc.* 35 (1939) 482; V. Vand, *Acta Cryst.* 9 (1959) 379.
- [66] C. A. Feldmann, R. Engelhardt, T. Permien, E. E. Koch, and V. Saile, *Nucl. Instrum. Methods* 208 (1983) 785.
- [67] C. N. Berglund and W. E. Spicer, *Phys. Rev.* 136A (1964) 1030.
- [68] For a summary, see e.g. D. Bloor, *Chem. Phys. Lett.* 40 (1976) 323.
- [69] N. Ueno unpublished.
- [70] M. Lösche and H. Möhwald, *Eur. Biophys. J.* 11 (1984) 35; *Colloid Surf.* 10 (1984) 217.
- [71] T. Fukui, M. Sugi, and S. Iizima, *Phys. Rev.* B22 (1980) 4898; T. Fukui, A. Matsuda, M. Sugi, and S. Iizima, *Bull. Electrotech. Lab.* 41 (1977) 423 (in Japanese).
- [72] H. Ozaki, Y. Harada, H. Nakahara, and K. Fukuda, *Proc. 2nd Int. Conf. Langmuir-Blodgett Films, Schenectady* (1985).
- [73] M. P. Seah and W. A. Donch, *Surf. Interf. Anal.* 1 (1979) 2.
- [74] L. Laxhuber, *Diplom. Thesis, Technische Universität München*, 1983.

- [75] For example, F. J. Himpsel, D. E. Eastman, E. E. Koch, and A. R. Williams, *Phys. Rev.* B22 (1980) 4604.
- [76] C. Kittel, *Introduction to Solid State Physics*, 5th ed. (Wiley, New York, 1976), Chapter 9.
- [77] J. J. Fireaux, R. Candano, and J. Verbist, *J. Electron Spectrosc.* 5 (1974) 267.
- [78] N. Ueno unpublished.
- [79] For example, E. Heilbronner and H. Bock, *Das HMO-Modell und seine Anwendung* (Verlag Chemie, Weinheim, 1970).
- [80] K. Seki, U. O. Karlsson, R. Engelhardt, E. E. Koch and W. Schmidt, *Chem. Phys.* 91 (1984) 459.
- [81] K. Seki, Y. Harada, and H. Inokuchi, *Chem. Phys. Letters* 20 (1973) 197.
- [82] S. Kiyono, N. Ueno, and Y. Hayashi, *Tech. Rep. Tohoku Univ.* 38 (1973) 173.
- [83] W. D. Grobman and E. E. Koch, in: *Photoemission in Solids*, Vol. 2, eds. L. Ley and M. Cardona (Springer, Berlin, 1979), p. 261.
- [84] C. E. Duke, *Surf. Sci.* 70 (1978); *Mol. Cryst. Liq. Cryst.* 50 (1979) 63.
- [85] F. Gutmann and L. E. Lyons: *Organic Semiconductors* (Wiley, New York, 1967).
- [86] K. Toriyama, K. Nunome, and M. Iwasaki, *J. Chem. Phys.* 77 (1982) 5891.
- [87] K. Seki, Y. Harada, K. Ohno, and H. Inokuchi, *Bull. Chem. Soc. Jpn.* 47 (1974) 1608.
- [88] W. R. Salaneck, *Phys. Rev. Lett.* 40 (1978) 60.
- [89] (a) W. D. Grobman, R. A. Pollak, D. E. Eastman, E. T. Maas-Jr., and B. A. Scott, *Phys. Rev. Lett.* 32 (1974) 534, (b) P. Nielsen, A. J. Epstein, and D. J. Sandman, *Solid State Commun.* 15 (1974) 53.
- [90] H. J. Stolz, PhD Thesis, Univ. Stuttgart (1977) cited in Ref. [83].

Table 2. Comparison of the observed and calculated valence energy structure of polyethylene (in eV).  
 All calculations are for an isolated extended planar-zigzag chain.

Authors	Ref.	Upper band ( $C_{2p} + H_{1s}$ )			Lower band ( $C_{2s}$ )			Total Valence Band Width	Remark			
		Top Peaks	Bottom	Width	Top Peaks	Bottom	Width					
Experiment This work	8.8 14.0 14.8	10.4	15.5	6.7	2.0	17.5	18.1	24.7	7.2	16.2	Solid state values <sup>e)</sup>	
Ab Initio												
André, Leroy	[4]	16.88 <sup>b)</sup>	—	20.41	3.53	6.53	26.94	—	33.47	6.53	—	wrong geometry
André, Kapssemens, Leroy	[8]	13.31	—	—	—	—	—	—	33.47	—	20.16	—
Clementi	[10]	12.84	—	(20.1)	(7.3)	(6.1)	(26.2)	—	(32.3)	(6.1)	19.5	wrong geometry
André, Delhalle, Delhalle, Caudano, Pireaux, Verbiest	[19]	—	13.46	—	—	—	—	26.81	—	—	—	—
			15.53	—	—	—	—	33.37	—	—	—	—
			17.61	20.19	—	—	—	—	—	—	—	—
			20.19	—	—	—	—	—	—	—	—	—
Delhalle, André, Delhalle, Pireaux, Caudano, Verbiest	[22]	13.2	—	(20.2)	7.0	6.0	(26.2)	—	(33.7)	7.5	—	—
Delhalle, Delhalle, André	[23]	—	—	—	—	—	—	—	—	—	—	same as Ref. [4]
Armstrong, Jamieson, Perkins	[31]	10.45	—	(17.3)	(6.9)	(4.9)	(22.2)	—	(30.2)	(8.0)	—	—
Karpfen	[38]	10.0	(10.1)	(17.6)	7.6	3.0	(20.6)	(20.9)	(29.3)	8.7	19.3	—
			(12.0)	—	—	—	—	—	—	—	—	—
			(15.1)	—	—	—	—	—	—	—	—	—
			(17.4)	—	—	—	—	—	—	—	—	—
Weidman, Bedford, Kunz	[39]	(14.2)	—	(19.6)	(5.4)	(3.3)	(22.9)	—	(25.3)	(2.4)	(11.1)	(CH <sub>2</sub> ) <sub>6</sub> (not an infinite chain)
Teramoe, Yamabe, Imamura	[40]	9.91	—	(18.9)	(9.0) <sup>c)</sup>	(2.8)	(21.7)	—	(30.3)	(6.6)	(20.4)	—
Teramoe, Yamabe, Imamura	[40]	11.05	—	(19.7)	(9.7) <sup>c)</sup>	(2.3)	(22.0)	—	(30.2)	(8.2)	(19.1)	—

continued

Table 1. Binding Energies of Spectral Features for Linear Chain Molecular Solids Relative to the Vacuum Level (in eV).

Compound and Method	Upper Band ( $C_{2s} + H_{1s}$ )				Lower Band ( $C_{2s}$ )			Ref.
	X	A	B	C	D <sup>a)</sup>	D	E	
n-C <sub>36</sub> H <sub>74</sub> and Cd arachidate Solid ARUPS		10.4	14.0	14.8	~17.1	18.1	24.1	this work
		+0.2	+0.3	+0.5		+0.2	+0.3	
n-C <sub>36</sub> H <sub>74</sub> Solid ARUPS		10.5 <sup>b)</sup>	14.0	15.5		18.3	24.6	[47]
		to 12.0						
Polyethylene <sup>c)</sup> Solid XPS	9.6	11.2	12.6	13.8		18.0	23.6	[22]
n-C <sub>36</sub> H <sub>74</sub> <sup>c)d)</sup> Solid XPS	9.8	11.1	13.7	15.4		18.0	23.8	[43,77]

a) Extrinsic feature observed for long-irradiated samples. See text.

b) Depends on the parameters of angle-resolved measurements.

c) Converted from the values relative to the Fermi level by using a value of 4.8 eV for the work function (see text).

d) Binding energies have been read from the spectrum.

Table 2 (continued)

CNDO	André, Kapsomenos, Leroy	[8]	11.70	—	—	—	—	—	[48.5]	—	36.84	
CNDO/2	Morokuma	[5]	(11.5)	—	(29.0)	(17.5)	—	—	(47.7)	—	(36.2)	crossing <sup>d)</sup>
	Fujita, Imamura	[7]	(11.7)	—	(29.3)	(17.6)	—	—	(48.0)	—	(36.2)	crossing <sup>d)</sup>
	Morokuma	[9]	(11.6)	—	(29.1)	(17.5)	—	—	(48.0)	—	(36.4)	crossing <sup>d)</sup>
	André, Delhalle, Kapsomenos, Leroy	[14]	(11.1)	—	(29.3)	(18.2)	0	(25.6)	(48.5)	(22.9)	(37.4)	
	Delhalle, André, Delhalle, Pireaux, Caudano, Verbist	[22]	11.7	—	(30.0)	(18.3)	0	(26.2)	(48.8)	22.6	31.1	
Modified CNDO	Morosi, Simonetta	[11]	(13.1)	—	(26.4)	(13.3)	—	—	(40.8)	—	(27.7)	crossing <sup>d)</sup> split at X point <sup>e)</sup>
	McAloon, Perkins	[15]	(4.9)	—	(40.0)	(35.1)	0	(29.7)	(84.7)	(55.0)	(79.8)	split at X point <sup>e)</sup>
	Wood, Barber, Hillier, Thomas	[16]	(11.0)	—	(20.2)	(9.2)	(1.3)	(21.5)	(33.7)	(12.2)	(22.7)	
	Delhalle, André, Delhalle, Pireaux, Caudano, Verbist	[22]	(9.6)	—	(20.1)	(10.5)	(1.0)	(21.1)	(32.6)	(11.5)	(23.0)	
	Perkins, Marwaha, Stewart	[34]	9.07	—	(16.4)	(7.3)	(2.9)	(19.3)	(29.3)	(10.0)	(20.2)	
INDO	Beveridge, Jano, Ladik	[13]	(9.6)	—	(29.2)	(19.6)	(6.2)	(25.8)	(48.8)	(23.0)	(39.2)	split at X point <sup>e)</sup>
MINDO/2	Beveridge, Jano, Ladik	[13]	—	—	—	—	—	—	—	—	—	
	Beveridge, Wun	[20]	(7.0)	—	(18.4)	(11.4)	(0.8)	(19.2)	(41.0)	(21.8)	(34.0)	split at X point <sup>e)</sup>
MINDO/3	Dewar, Suck, Weiner	[18]	(8.3)	—	(16.0)	(7.7)	(3.3)	(19.3)	(36.8)	(17.3)	(28.5)	peak energies are from Refs. [30] and [33]
MNDO	Dewar, Yamaguchi, Suck	[30]	(11.0)	10.9 12.3 14.7 17.1	(17.2)	6.2	5.2	(22.4)	22.3 41.4	(41.4)	19.0	40.4

continued

37

Table 2 (continued)

	Dewar, Yamaguchi, Suck	[33]	(11.0)	11.0 12.1 12.4 17.2	(17.2)	6.2	5.5	(22.7)	22.7 41.5	(41.5)	18.8	30.5	
Extended Hückel	McCubbin, Manne	[3]	(12.4)	—	(17.0)	(4.6)	(2.9)	(19.9)	—	(28.7)	(8.8)	(16.3)	
	Imamura	[6]	12.05	—	16.94	[4.89]	[2.93]	[19.87]	—	[28.85]	[8.98]	[16.8]	
	André, Kapsomenos, Leroy	[8]	12.05	—	—	—	—	—	—	28.85	—	16.82	
	Delhalle, André, Delhalle, Pireaux, Caudano, Verbist	[22]	11.9	—	[17.4]	5.5	2.5	[19.9]	—	[29.4]	9.5	[17.5]	
	Delhalle, Delhalle, Damanet, André	[24]	12.05	—	16.94	[4.89]	[3.0]	[19.94]	—	[28.85]	[8.91]	[16.8]	
SANO	Duke, O'Leary	[17]	12.76	—	(19.7)	(6.9)	(7.0)	(26.7)	—	33.28	(6.6)	20.52	
FSGO	Bredas, André, Delhalle	[35]	(8.7)	—	(15.1)	(6.4)	(6.4)	(17.1)	—	(23.7)	(6.6)	(15.0)	
LCLO	Dyachkov, Levin	[26]	10.2	—	—	—	—	—	—	(25.7)	—	(15.5)	split at X point <sup>e)</sup>
	Dyachkov, Iosolovich, Levin	[27]	(10.6)	—	(16.9)	(6.3)	(2.1)	(19.0)	—	(25.8)	(6.8)	(15.2)	
	Armstrong, Jamieson, Perkins	[36]	7.81	—	[14.37]	6.56	(7.5)	(21.9)	—	(31.8)	(9.9)	(24.0)	
	Leroy, Peeters, Resoux-Clarisse	[28]	13.03	—	20.32	7.29	[1.84]	22.16	—	32.16	9.48	19.13	
	Delhalle, André, Delhalle, Pivont-Malherbe, Clarisse, Leroy, Peeters	[29]	13.17	—	[19.95]	6.78	[2.67]	[22.62]	—	[32.05]	9.44	18.88	
LCAO-MO	Falk, Fleming	[18]	11.3	—	(22.6)	11.3	1.0	(23.6)	—	(29.2)	(5.6)	17.9	
EMTO	Kasowski, Hsu, Caruthers	[37]	12.8	—	18.4	5.6	[2.2]	20.6	—	27.6	7.0	14.8	Bands are not flat at $\Gamma$ Point
DV-X $\alpha$	Satoko	[41]	12.73	—	17.55	4.81	[2.56]	20.11	—	29.26	9.14	16.53	

Notes are in the following page.

38

Remarks to Table 2.

[ ]: derived from numerical values in the literature.

( ): read from figures.

a) For comparison with calculations, a solid-state shift of  $\sim 0.5$  eV should be added. For details, see text.

b) This value listed by the authors is inconsistent with the figure in the same paper. A value of 13.31 eV in Ref. [8] seems more reasonable.

c) The value listed by the authors is inconsistent with the figures in the same paper.

d) There is a crossing of bands of the same symmetry, which should be split to avoid the crossing [12,25].

e) The rule of pairing at the edge of the Brillouin zone (X-point) is not fulfilled [18a].

#### Figure Captions

Fig. 1. Schematic structure of the evaporated film of hexatriacontane (a), the Langemuir-Blodgett films of Cd arachidate for two layers and three layers (b), and the crystal of polyethylene [65](c). For both cases of (b), the upper 20 Å layer consists of oriented hydrocarbon chains. Due to the hydrophobic nature of Au and hydrophilic character of Al, even or odd numbers of monolayers can be deposited, respectively.

Fig. 2. (a) Parameters of angle-resolved UPS measurements:  $\alpha$ , incidence angle of photon,  $\theta$ , polar emission angle of electrons, and  $\phi$ , azimuthal emission angle of electrons. (b) Schematic  $E = E(k)$  bands. A direct transition between an initial band  $E_i$  and a final band  $E_f$  is depicted.

Fig. 3. Photoelectron energy distribution curves at normal emission to the surface ( $\theta = 0^\circ$ ) of hexatriacontane for photon energies ranging from 22 eV to 45 eV. In this plot the same initial states follow inclined lines.

Fig. 4. (a) Normal-emission spectra of hexatriacontane for  $h\nu = 38$  eV for different angles of incidence of photons  $\alpha$ .  
(b) Dependence of the hexatriacontane photoelectron spectra for  $h\nu = 38$  eV and  $\alpha = 70^\circ$  on the emission angle of electrons  $\theta$ .  
(c) Comparison of the photoelectron energy distribution curves of an evaporated film of n-C<sub>36</sub>H<sub>74</sub> and 2- and 3-layer LB films of Cd arachidate for  $\alpha = 70^\circ$ ,  $\theta = 0^\circ$ ,

and  $h\nu = 38$  eV. The ratio of the peak intensities A to D is given for each spectrum.

- Fig. 5. Change of the photoelectron spectra of Cd arachidate for  $h\nu = 38$  eV and two different emission angles  $\theta$  ( $0^\circ$  and  $60^\circ$ ) by heat treatment at  $100^\circ\text{C}$ . Lower panel: before heat treatment; upper panel: after heat treatment. Note the disappearance of the  $\theta$ -dependence after heat treatment.
- Fig. 6. Photon-energy dependence of the normal-emission spectra of hexatriacontane for  $\alpha = 70^\circ$ . Arrows indicate the location of the spectral features.
- Fig. 7. Photon-energy dependence of the normal-emission spectra of 2 layers LB film of Cd arachidate for  $\alpha = 70^\circ$ . Arrows indicate the location of the spectral features.
- Fig. 8. Photon-energy dependence of the intensity of the upper  $\text{C}_{2s}$  derived band (D) for Cd arachidate.
- Fig. 9. Illustration of the nearly-free-electron like final-state energy dispersion (I - III) used for the analysis and the transition corresponding to the intensity maximum of peak D in Fig. 8. The dispersion of the initial states is taken from Karpfen [38] with modifications described in the text.
- Fig. 10. Summary of the intramolecular energy band dispersion data for the valence bands of hexatriacontane and Cd arachidate.
- : from  $\alpha = 70^\circ$  measurements using evaporated  $n\text{-C}_{36}\text{H}_{74}$  film.

○: from  $\alpha = 70^\circ$  measurements using 2 layers LB film of Cd arachidate.

□: from  $\alpha = 70^\circ$  measurements using 3 layers LB film.

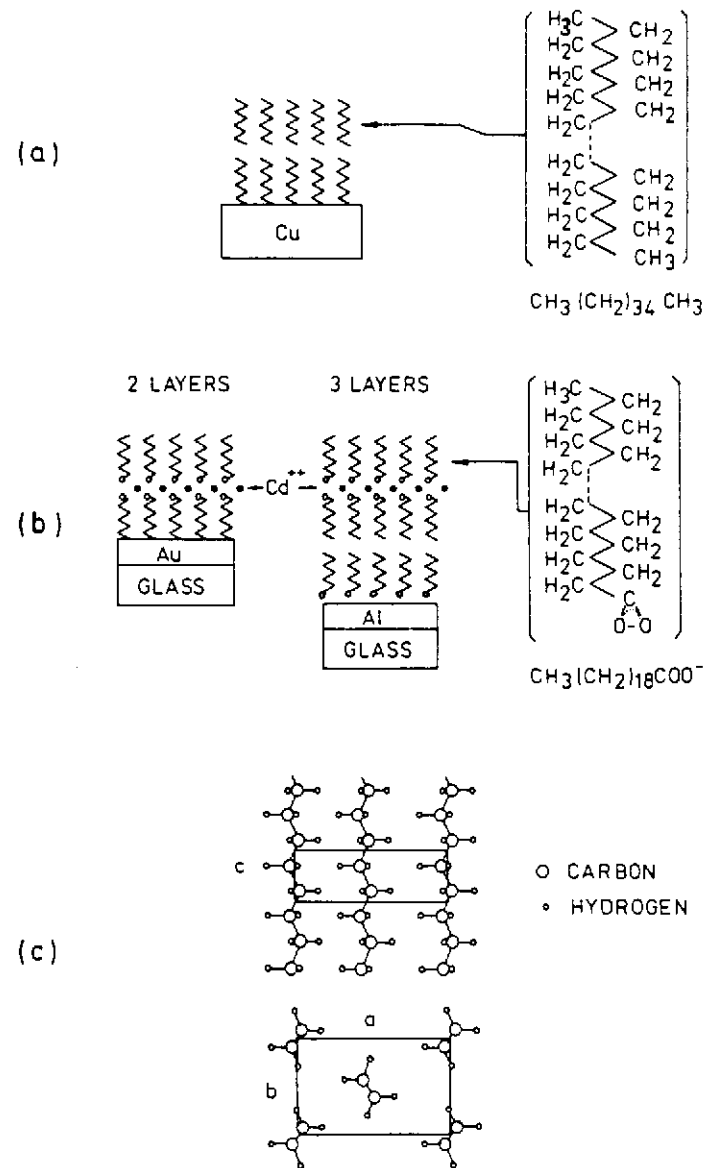
△: from  $\alpha = 80^\circ$  measurements using 3 layers LB film.

The calculated band structure for idealized polyethylene (broken line) is a modification of the results by Karpfen [38] (see text). The lack of the experimental points near the X point ( $k = \pi/a$ ) is only due to the limitation of available photon energy by the Seya-Namicka monochromator.

- Fig. 11. Comparison of the UPS spectra of hexatriacontane (a) and Cd arachidate (b) with the XPS spectra of polyethylene [22] and hexatriacontane [43,77] (c). For details, see text.
- Fig. 12. Energy band dispersion of the  $\text{C}_{2s}$  band of polyethylene derived from XPS results of alkane oligomers for (○) from methane to pentane in the gas phase [43], and (●) from pentane to nonane in the solid state [44], using Eq. (7). Bars indicate the direction of possible error in separating multiple components in a single observed spectral feature. The calculated energy-band dispersion is the same as in Fig. 10.
- Fig. 13. Comparison of the experimentally observed  $E = E(k)$  relation (● in (a) and (e), this work) with theoretical calculations.
- (a) ab-initio method [38], (b) CNDO/2 method [22], (c) Modified CNDO/2 method [34], (d) MNDO method [33], (e) Extended Hückel method (Wolfsberg-Helmholtz parameter F

= 1.75) [3], (f) FSGO method [35], and (g) LCAO-MT method [18]. The energy axis of (a) is not modified as in Figs. 9 and 10. The energy scale of the experimental data in the right ordinates of (a) and (e) are shifted to show a good agreement with calculations.

Fig. 14. Comparison of the calculated density of states for polyethylene ((a) - (g)) with UPS and XPS spectra of hexatriacontane and Cd arachidate. For XPS, we preferred the spectrum of hexatriacontane [77] to that of polyethylene due to the reason described in the text.





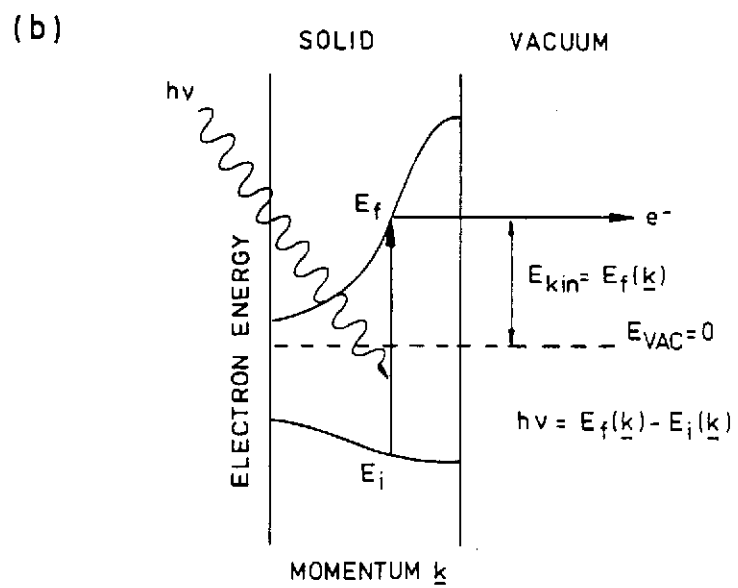
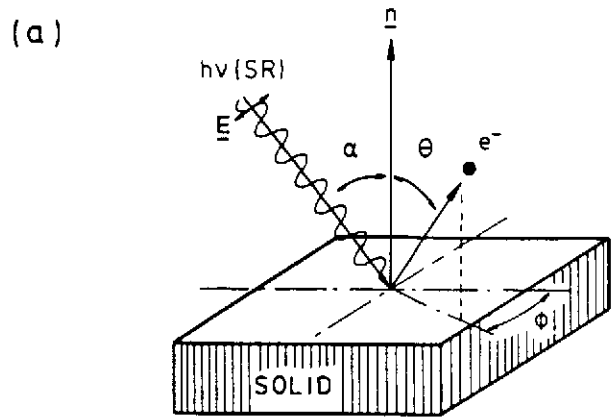


Fig. 2

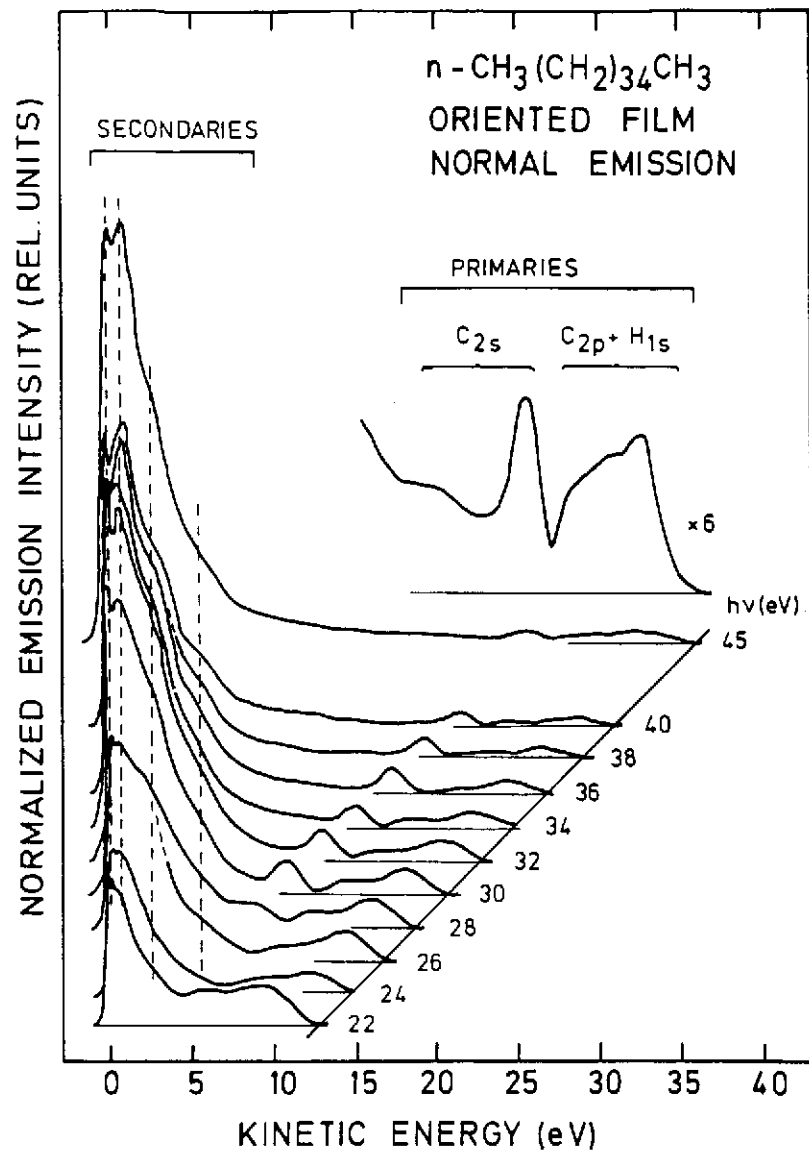
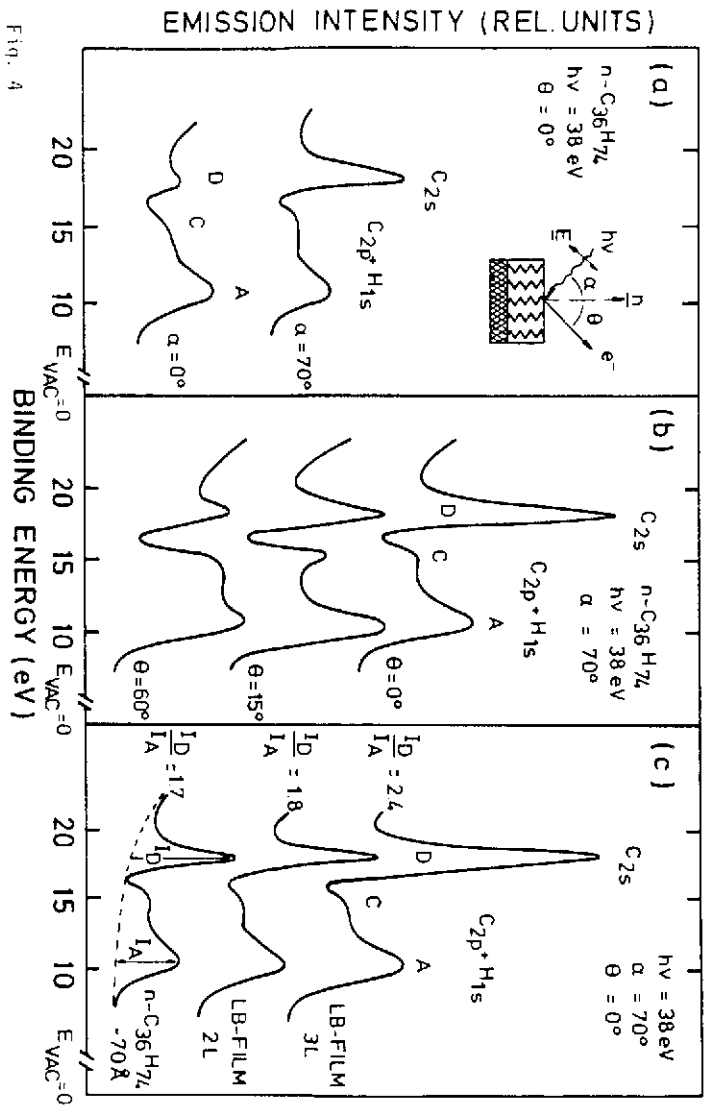


Fig. 3

Fig. 4



EMMISSION INTENSITY (REL. UNITS)

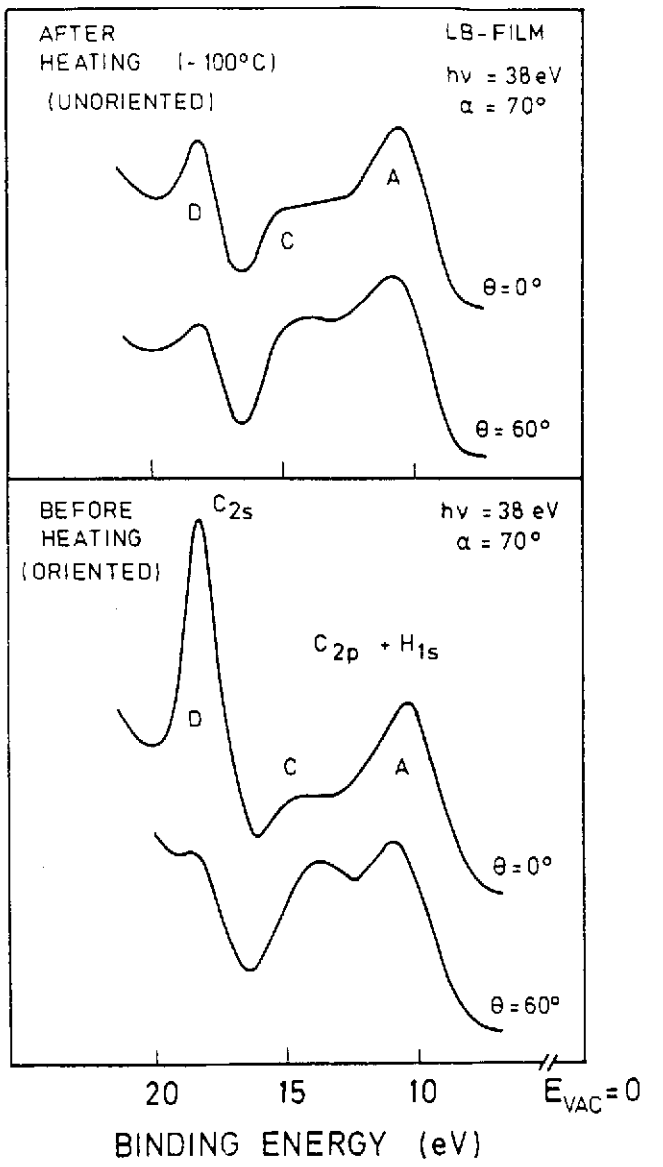


Fig. 5

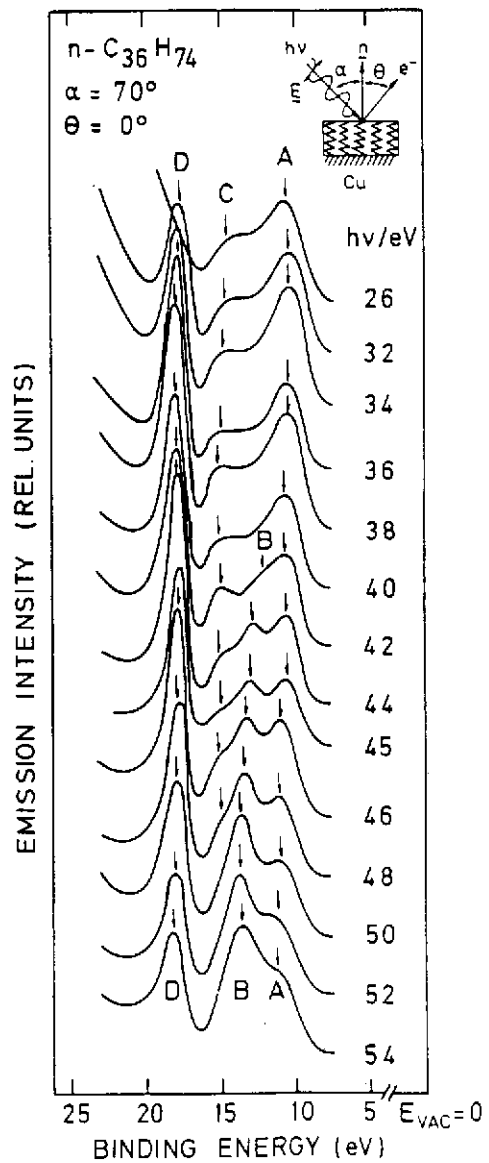


Fig. 6

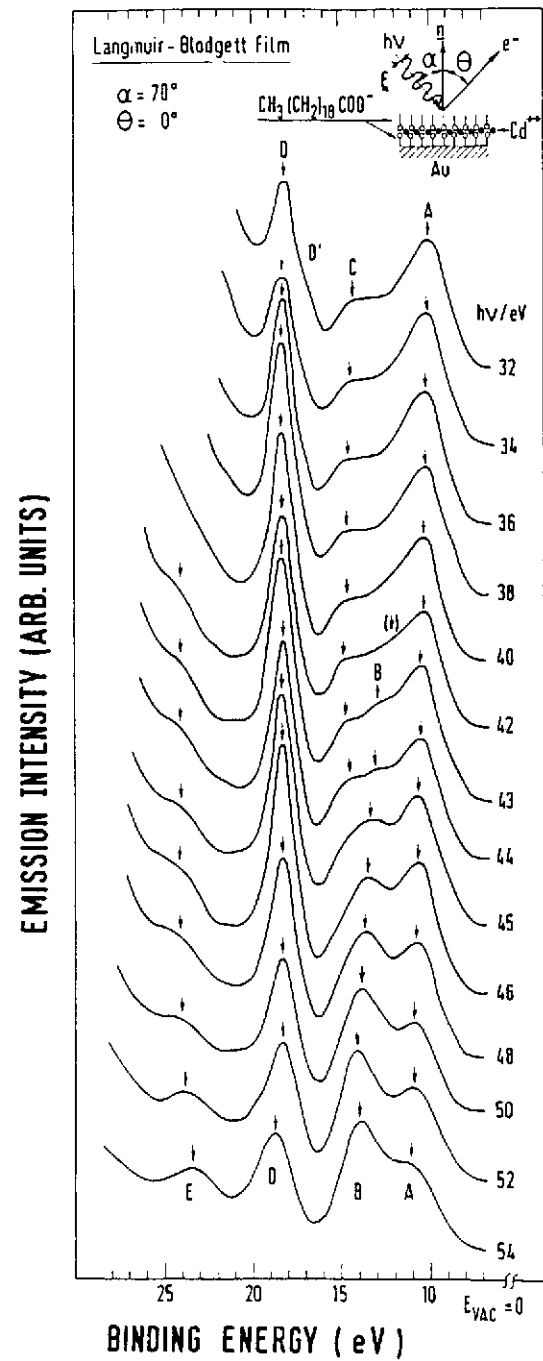


Fig. 7

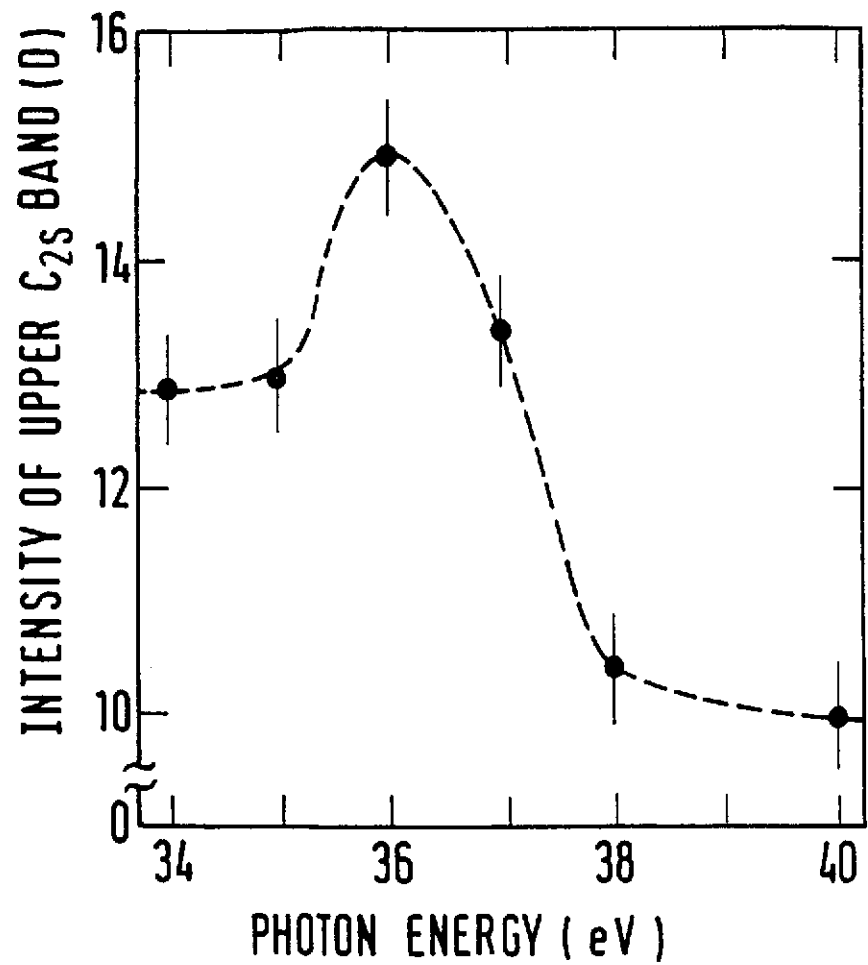


Fig. 8

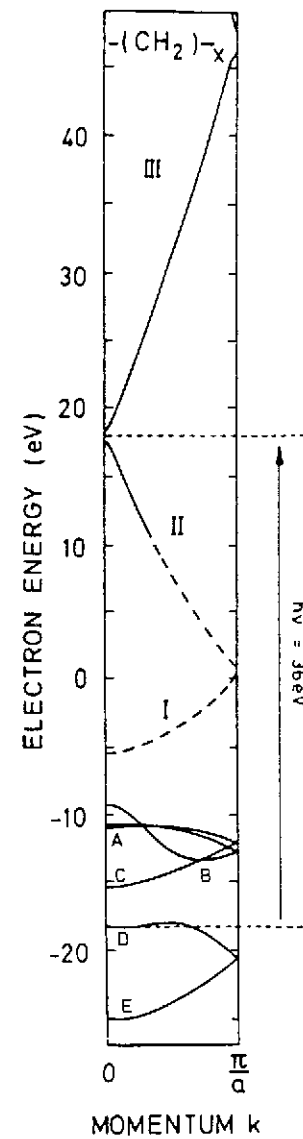


Fig. 9

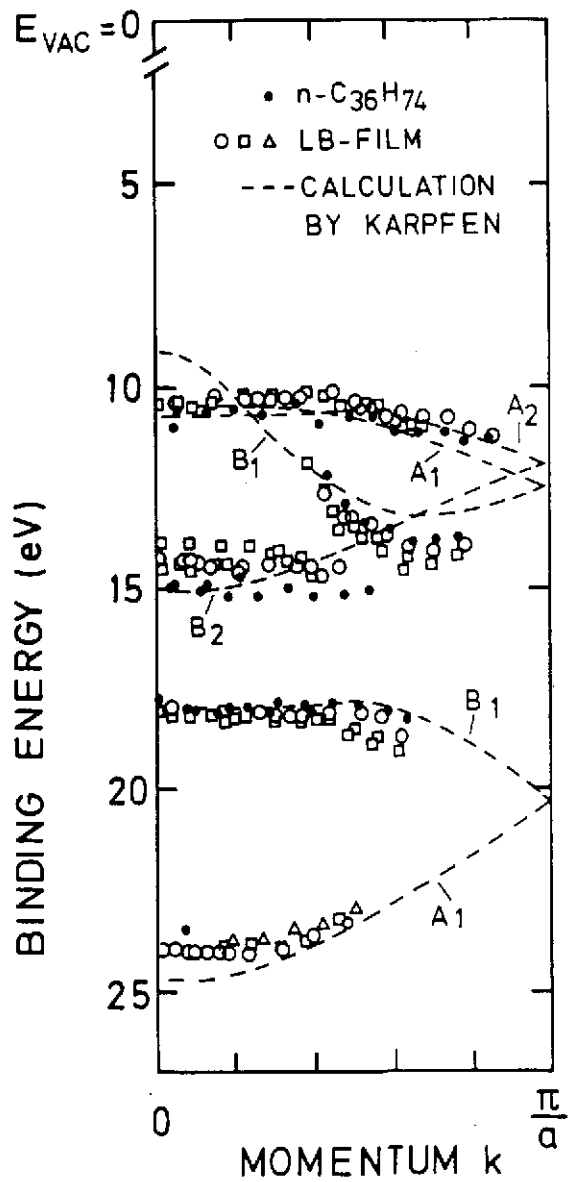


Fig. 10

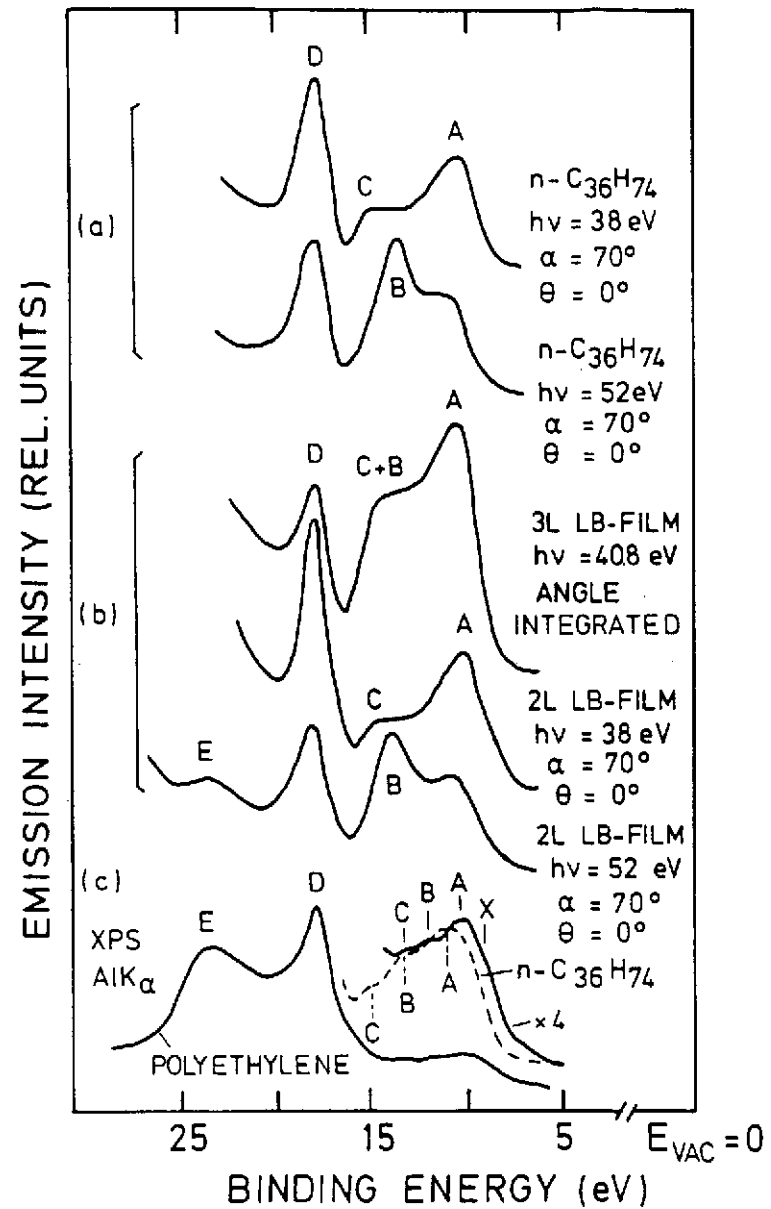


Fig. 11

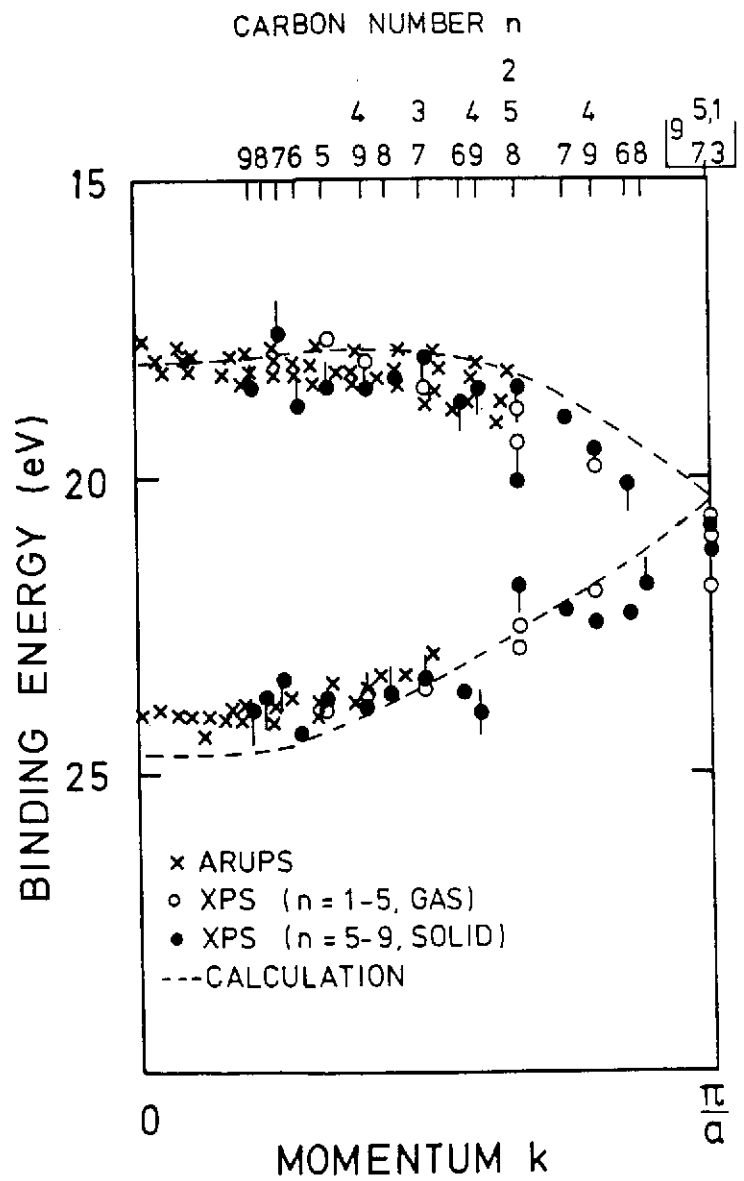
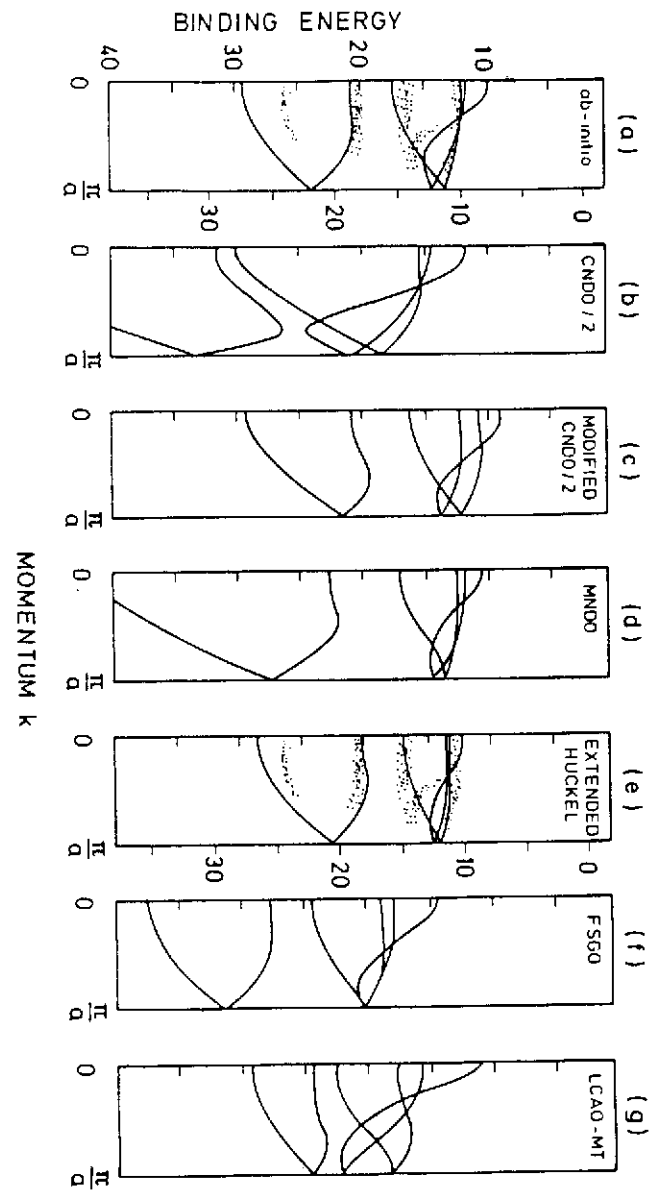


Fig. 12

Fig. 13



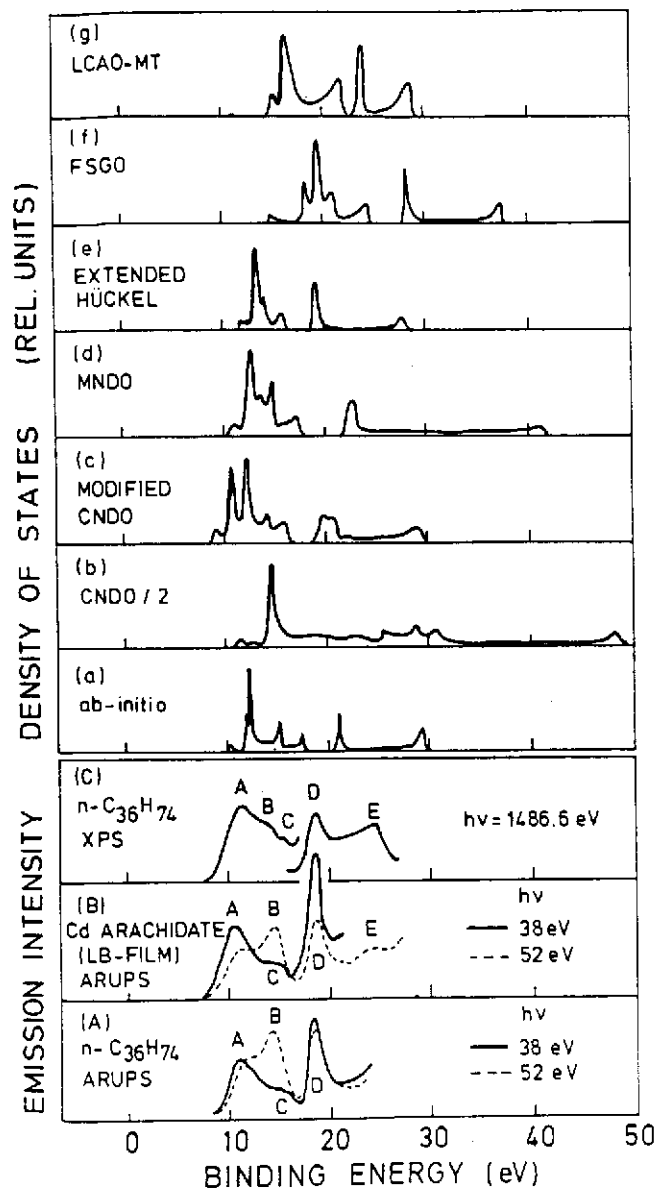


Fig. 14

